JRMP Journal of Radiopharmaceuticals and Molecular Probes Vol. 2, No. 2, 2016
J Radiopharm Mol Probes 2016;2(2):73-83
ISSN 2384-1583(Print) / ISSN 2508-3848(Online)

REVIEW

https://doi.org/10.22643/JRMP.2016.2.2.73

[^{18}F]Labeled 2-nitroimidazole derivatives for hypoxia imaging

Sudhakara Reddy Seelam[1-3], Yun-Sang Lee[1,2], Jae Min Jeong[1-3*]

[1] Department of Nuclear Medicine, Institute of Radiation Medicine, Seoul National University College of Medicine, Seoul, Republic of Korea
[2] Cancer Research Institute, Seoul National University College of Medicine, Seoul, Republic of Korea
[3] Department of Radiation Applied Life Science, Seoul National University College of Medicine, Seoul, Republic of Korea

ABSTRACT

Imaging hypoxia using positron emission tomography (PET) is of great importance for cancer therapy. [^{18}F] Fluoromisonidazole (FMISO) was the first PET agent used for imaging tumor hypoxia. Various radiolabeled nitroimidazole derivatives such as [^{18}F]fluoroerythronitroimidazole (FETNIM), [^{18}F]1-α-D-(2-deoxy-2-fluoroarabinofuranosyl)-2-nitroimidazole(FAZA), 2-(2-nitroimidazol-1-yl)-N-(3,3,3-[18F]-trifluoropropyl)acetamide ([^{18}F]EF-3), [^{18}F]2-(2-nitro-1H-imidazol-1-yl)-N-(2,2,3,3,3-pentafluoropropyl) acetamide (EF-5), 3-[^{18}F]fluoro-2-(4-((2-nitro-1H-imidazol-1-yl)methyl)-1H-1,2,3,-triazol-1-yl)-propan-1-ol ([^{18}F]HX-4), and [^{18}F]fluoroetanidazole (FETA) were developed successively. However, these imaging agents still produce PET images with limited resolution; the lower blood flow in hypoxic tumors compared to normoxic tumors results in low uptake of the agents in hypoxic tumors. Thus, the development of better imaging agents is necessary.

J Radiopharm Mol Probes 2(2):73-83, 2016

Key Word: [^{18}F]FMISO, 2-nitroimidazole, PET, fluorine-18, hypoxia

Introduction

Positron emission tomography (PET) is a nuclear imaging technique used in the diagnosis of different types of cancer, such as colorectal cancer, melanoma, head and neck cancer, lung cancer, breast cancer, and prostate cancer, because of its wide scope and high sensitivity (1-7). ^{18}F ($t_{1/2}$ = 109.77 min, 90% β+, $E_{\beta+max}$ = 0.635 MeV, 3% EC) is the most commonly used PET radioisotope because of excellent imaging properties, and thus, the development of ^{18}F-labeled bioactive molecules has become an important area.

Several radiolabeled 2-nitroimidazole derivatives, such as [^{18}F]fluoromisonidazole ([^{18}F]FMISO) (8, 9), [^{18}F]fluoroerythronitroimidazole ([^{18}F]FETNIM) (10), 1-R-D-(2-deoxy-2-[^{18}F]fluoroarabinofuranosyl)-2 nitroimidazole ([^{18}F]-FAZA) (11), 2-(2-nitroimidazol-1-yl)-N-(3-[^{18}F]fluoropropyl)acetamide ([^{18}F]-EF1) (12), 2-(2-nitroimidazol-1-yl)-N-(3,3,3-[^{18}F]-trifluoropropyl) acetamide ([^{18}F]EF-3) (13), 2-(2-nitro-1H-imidazol-1-yl)-N-(2,2,3,3,3-[^{18}F]-pentafluoropropyl) acetamide ([^{18}F] EF-5) (14), 3-[^{18}F]fluoro-2-(4-((2-nitro-1H-imidazol-1-yl) methyl)-1H-1,2,3,-triazol-1-yl)-propan-1-ol ([^{18}F]HX-4) (15), and [^{18}F]-fluoroetanidazole ([^{18}F]FETA) (16) have been developed and extensively studied to detect tumor hypoxia. Nitroimidazole residue is reduced to reactive chemical species, which can bind to cell components in the absence of sufficient oxygen (11, 17-22).

Among them, [^{18}F]FMISO was most widely used nitroimidazole derivate for imaging tumor hypoxia in

November 18, 2016 / Revised: December 14, 2016 / Accepted: December 17, 2016

Correspnding Author : Jae Min Jeong, Ph.D./Department of Nuclear Medicine Seoul National University Hospital 101 Daehangno Jongno-gu, Seoul 03080 Korea
E-mail: jmjng@snu.ac.kr / Tel: +82-2-2072-3805, Fax: +82-2-745-76

vivo with clinical PET (23, 24). [^{18}F]FMISO has been shown to selectively bind to hypoxic cells both in vitro and in vivo. [^{18}F]FMISO has favorable chemical and physicochemical properties in terms of lipophilicity (octanol/water partition coefficient; log P = 2.6) and an appropriate reduction potential of E-389 mV that are responsible for high cellular uptake and trapping in hypoxic cells (25, 26). Many other nitroimidazole derivatives have been developed and used for pre-clinical and clinical tests(Figure 1).

Recently, Al^{18}F-labeled 1, 4, 7-triazacyclononane-1,4-diacetic acid (NODA)-nitroimidazole derivatives (2,2'-(7-(2-(2-nitroimidazolyl)ethyl)-1,4,7-triazonane-1,4-diyl)diacetic acid (1) and 2, 2'-(7-(3-(2-nitroimidazolyl) propyl)-1,4,7-triazonane-1,4-diyl)diacetic acid (2) have been reported. These conjugates showed higher standard uptake values (SUV) and tumor-to-muscle ratios than 1,4,7-triazacyclononane-1, 4, 7-triacetic acid (NOTA) and 1,4,7,10-tetraazacyclododecane-1, 4, 7,10-tetraacetic acid (DOTA) nitroimidazole derivatives (Figure 2) (27). This method offers straightforward ^{18}F labeling in aqueous solutions with high radiochemical yields (27-29).

This review looks at various ^{18}F-labeled 2-nitroimidazole derivatives for tumor hypoxia imaging and compares major parameters like percentage of injected dose per weight (% ID/g), tumor-to-blood (T/B), and tumor-to-muscle (T/M) ratios between established hypoxia markers in preclinical studies(Table 1).

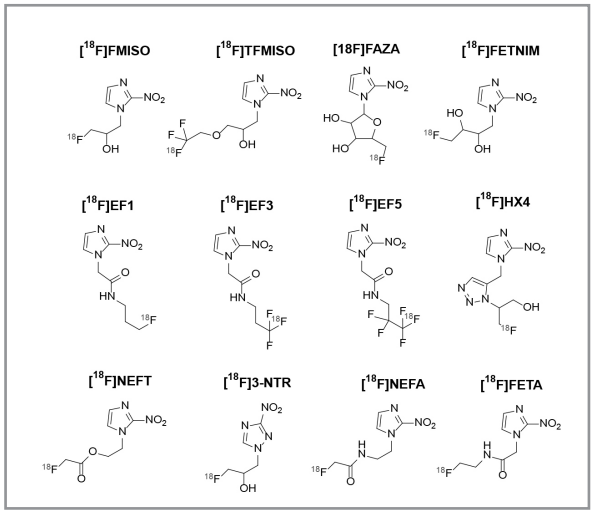

Figure 1. Structures of known 18F-labeled 2-nitroimidazole derivatives as hypoxia imaging agents.

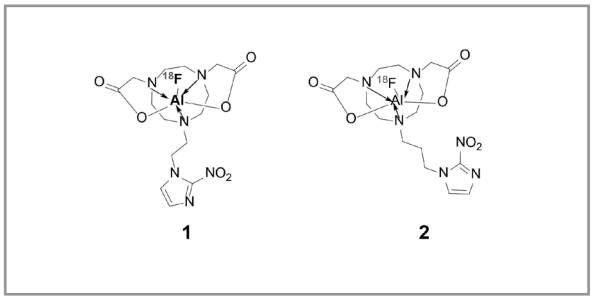

Figure 2. Structures of 18F labeled nitroimidazole derivatives that were developed recently. 1) 2,2'-(7-(2-(2-nitroimidazolyl)ethyl)-1,4,7-triazonane-1,4-diyl)diacetic acid (1); 2) 2,2'-(7-(3-(2-nitroimidazolyl)propyl)-1,4,7-triazonane-1,4-diyl)diacetic acid (2).

Table 1. Partition-coefficient values of 2-nitroimidazole based hypoxia imaging agents.

Name	Partition-coefficient Values	References
[^{18}F]FMISO	2.6	(11, 57)
[^{18}F]TFMISO	2.6	(47)
[^{18}F]FAZA	1.1	(11)
[^{18}F]FETNIM	0.17	(46, 47)
[^{18}F]EF-1	0.20	(47)
[^{18}F]EF-3	1.25	(47, 52)
[^{18}F]EF-5	5.7	(47, 52)
[^{18}F]HX-4	-0.69	(15, 56)
[^{18}F]FETA	0.16	(37)
[^{18}F]FRP-170	0.094	(56)
[^{18}F]NTR	–0.46	(51)

2-Nitroimidazole as hypoxic agent

2-Nitroimidazole, which is thought to be reduced and to accumulate at the sites of hypoxia, has been labeled with 18F, ^{123}I, and ^{99m} Tc and used for imaging purposes in both single photon emission computed tomography (SPECT) and PET.

In particular, 2-nitroimidazole can be reduced to form a reactive chemical species, which can bind irreversibly to cell components in the absence of sufficient oxygen; therefore, development of radiolabeled nitroimidazole derivatives for the imaging of tumor hypoxia remains an active field of research to improve cancer therapy results (17, 30-32). When a nitroimidazole molecule enters hypoxic cells, it undergoes an enzymatic single electron reduction, depending on the availability of oxygen, and forms several radical anions (33, 34). These anions undergo further reduction to produce nitroso ($2e^-$ reduction), hydroxylamine ($4e^-$ reduction), and amine ($6e^-$ reduction) derivatives(Figure 3). Furthermore, as a result of these processes, any radiolabeled species is selectively retained in hypoxic cells (19, 20, 22). The process is initiated by an enzyme-mediated (nitroreductase) single electron reduction to form a free radical. After the hypoxia-sensitive reduction of the nitro group to amine, ^{18}F-labeled nitroimidazoles are bound to intracellular proteins in the tumor (20).

The 4-nitroimidazoles (-527 mV) have a lower electron affinity and single electron reduction potential (SERP) value than the 2-nitroimidazoles (-389 mV), which means 2-nitroimidazoles are more efficiently reduced and retained in hypoxic cells than 4-nitroimidazoles (35, 36). The nitro group with appropriate redox potential (-380 to -390 mV), lipophilicity, stability to hypoxia independent degradation, and structure are important in determining the overall behavior of the hypoxia imaging agent (36, 37). For ^{18}F-based PET radiopharmaceuticals, high photon flux (and low energy) is needed for high detection sensitivity and spatial image resolution (37).

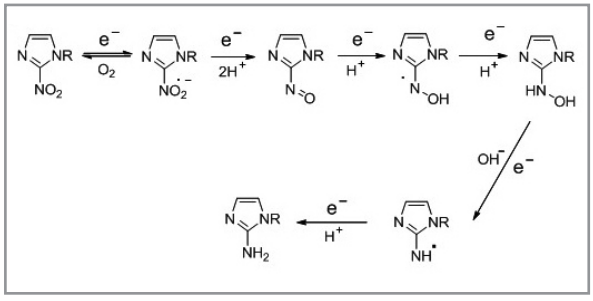

Figure 3. Proposed mechanism for nitroimidazole

^{18}F-labeled 2-nitroimidazoles

[^{18}F]FMISO was the first and most widely used 2-nitroimidazole agent used for in vivo hypoxia PET imaging (7, 38, 39). It has been evaluated extensively for the detection of tumor hypoxia pre-clinically using different animal models (Table 2). The first clinical study to image tumor hypoxia using [^{18}F]FMISO was conducted by Rasey et al (40). It was used to quantify the hypoxic fraction in patients with lung, head and neck, and prostate cancers (41, 42). It was also used in the hearts of patients with myocardial ischemia (43, 44). Several pre-clinical and clinical studies have shown its potential as a hypoxia imaging agent (45). It is cleared mainly through the hepatobiliary and gastrointestinal pathway (Table 2). Its highest activity was found in the liver and intestines, and percentages of intact [18F]FMISO in plasma, urine, kidney, and liver were 47%, 77%, 3%, and 3%, respectively (46). Because of the lipophilic nature of [^{18}F]FMISO, it failed to gain wider acceptance for routine clinical application. Several alternative nitroimidazole derivatives have been developed to improve the imaging performance by improving target to non-target ratio by increasing excretion rates and overcome some of the limitations of [^{18}F]FMISO such as nonspecific retention, metabolic conversion, and low partition coefficient, all leading to faster clearance properties (47).

[^{18}F]FAZA is another 2-nitroimidazole hypoxia imaging agent. The alkyl side chain in [^{18}F]FMISO is

replaced by a polar arabinose sugar in an attempt to increase the overall hydrophilicity of the compound (48). [^{18}F]FAZA was found to be able to diffuse rapidly through tissue and be excreted by the kidneys faster due to its highly hydrophilic nature (log P = 1.1) compared to [^{18}F]FMISO (log P = 2.6) (Table 1) (11). Accordingly, [^{18}F]FAZA was cleared more quickly from blood and normal tissues in animal studies and provided higher tumor-to-muscle ratios than [^{18}F]FMISO. Similar to [^{18}F]FMISO, [^{18}F]FAZA was found to be useful for imaging hypoxia in various tumors (Table 2) (47, 48). [^{18}F]FETA is also a 2-nitroimidazole analog that was found to have significantly lower levels of retention in the liver and lungs than [^{18}F]FMISO (16). [^{18}F] FETNIM also showed rapid elimination in non-target tissues via excretion through the urinary pathway (49). By introducing the 1,2,3-triazole moiety in [^{18}F]HX-4, its clearance properties improved relative to [^{18}F] FMISO, demonstrating that the kidney is the major [^{18}F]HX-4 excretion pathway (15). The low levels of uptake in intestines, liver, kidney, and other normal tissues result in lower background signals, which enhances the imaging properties of [^{18}F]HX-4 (15). 1-[^{18}F]Fluoro-3-(3-nitro-1H-1,2,4-triazol-1-yl)propan-2-ol ([^{18}F]NEFA) and 2-[^{18}F]Fluoro-N-(2-(2-nitro-1H-imidazol-1-yl)ethyl)acetamide ([^{18}F]NEFT) derivatives have been reported to have lower mean tumor uptakes ([^{18}F]NEFA: 1.55 ± 0.65; [^{18}F]NEFT: 2.45 ± 0.08; [^{18}F] FMISO: 3.29 ± 0.73) and lower tumor-to-muscle ratios ([^{18}F]NEFA: 1.14; [^{18}F]NEFT: 1.41; [^{18}F]FMISO: 1.74) than [^{18}F]FMISO in EMT-6 tumor-bearing mice at 30 min post-injection (Table 2) (50). 3-[^{18}F]Fluoro-2-(4-((2-nitro-1H-imidazol-1-yl)methyl)-1H-1,2,3-triazol-1-yl)propan-1-ol ([^{18}F]3-NTR) was developed, but because of its poor binding capabilities, it could not be used as a hypoxia marker (51). [^{18}F]3-NTR (1.5 ± 0.1) showed lower in vitro uptake than [^{18}F]FMISO (11.0 ± 0.4) in an HT1080 cell line 3 h post-incubation (Table 2) (51).

However, it might be difficult for more hydrophilic compounds to diffuse into tumor tissues and stay there (11, 38). Therefore, more lipophilic derivatives, such as [^{18}F]EF-3 and [^{18}F]EF-5, were developed (52). One possible disadvantage of [^{18}F]EF-3 and [^{18}F]EF-5 is that the labeling chemistry is more complex than the simple nucleophilic displacement reaction used for mono-fluorinated 2-nitroimidazoles (47). Animal models of these fluorinated derivatives showed a more homogeneous distribution in normal tissues along with clearance through the intestines and kidneys, and accumulation in hypoxic tumors (13, 14, 53, 54).

Hypoxic tumor uptake of the above mentioned tracers in xenograft-bearing mice demonstrated both high focal and more patchy distribution of the hypoxia PET tracer (55). These heterogeneous patterns of accumulation can be explained by the way the vascular structures, responsible for the tracer influx and washout, are organized within the tumor (15). The need to wait for several hours to permit clearance of the agent from the non-target tissues (contrast between lesion and background is typically < 2:1 at about 90 min post-injection), is a major drawback to ^{18}F labeled agents due to its short half-life of 110 min (17). Due to various limitations, none of these radiotracers have found their way into routine clinical use (37).

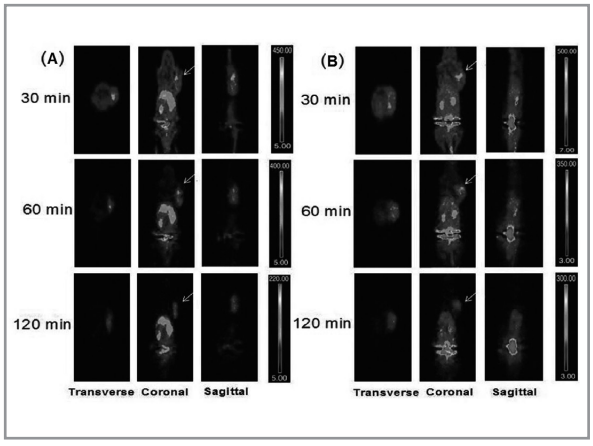

Figure 4. Small animal micro positron emission tomographic images of CT-26 tumor bearing mice at 30, 60, and 120 min after intravenous injection of (A) 1; and (B) 2. Arrows indicate the tumors. Reprinted with permission of the American Chemical Society from: Hoigebazar L et al., J Med Chem. 2012;55(7):3155.

Recently, an ^{18}F-labeling method using an Al^{18}F complex in aqueous solution was used as a straightforward ^{18}F-labeling procedure (28). 2-nitroimidazole derivatives conjugated with NODA that can be labeled with ^{18}F using an Al^{18}F complex. The synthesized derivatives had excellent ^{18}F-labeling efficiencies, high stabilities, and specific uptakes in cultured hypoxic tumor cells. These derivatives showed higher tumor to non-tumor ratios in xenograft-bearing mice (27) (Figure 4).

Although the uptakes of various ^{18}F-nitroimidazole compounds in tumors have been reported before, it is difficult to compare them because of different animal models, nature of the tumors induced, and post-injection times. Thus, a comparison of major parameters (%ID/g, T/B, T/M, and major clearance organs) between established hypoxia markers in preclinical studies was made in Table 2. The imaging studies to visualize tumor hypoxia in human subjects of the tracers mentioned above have been reviewed in several studies (18, 38, 56).

Conclusion

Imaging hypoxia is very important to improve cancer therapy results; therefore, developing hypoxia imaging agents have become an active part of research. Many nitroimidazole and non-nitroimidazole derivatives have been developed for detecting hypoxia, but only a few are used for clinical studies. PET using the 2-nitroimidazole [^{18}F]FMISO holds promise for the evaluation of tumor hypoxia at both global and local levels. Many other derivatives have been developed for imaging hypoxia, which have provided better results and may potentially replace [^{18}F]FMISO.

Table 2. Comparison of major parameters (% ID/g, T/B, and T/M) between established hypoxia markers in preclinical studies.a

Animal model	Tumor type	% ID/g	T/B	T/M	Clearance organs	References.
[^{18}F]-FMISO						
BALB/c nude mice	A549 human NSCLC			3.5		(58)
BALB/c nude mice	NCI-H520 human NSCLC			4.45		(58)
BALB/c nude mice	NCI-H596 human NSCLC			2.59		(58)
BALB/c nude mice	U87 MG human glioblastoma			1.93		(58)
BALB/c nude mice	PC3 human prostate			3.53		(58)
BALB/c nude mice	DU145 human prostate			2.27		(58)
BALB/c nude mice	Caki human RCC			1.28 ± 0.36		(58)
BALB/c nude mice	SK-N-BE human neuroblastoma			2.48		(58)
BALB/c nude mice	CLS-2 human urinary bladder carcinoma			3.62 ± 0.06		(58)
BALB/c nude mice	KB-31 human nasopharyngeal carcinoma			5.7		(58)

Swiss nude mice	A431 human epidermoid carcinoma	3.67 ± 1.00 (3 h)	4.92 ± 0.77 (3 h)	3.95 ± 1.34 (3 h)	Liver-kidney-intestines	(57)
BALB/c	B16 mouse melanoma			2.04 ± 0.83 (90 min)		(58)
Swiss nude mice	AR42J rat pancreatic acinar carcinoma	2.27 ± 0.39 (3 h)	3.39 ± 0.52 (3 h)	2.92 ± 0.66 (3 h)	Liver-kidney-intestines	(57)
BALB/c mice	EMT6 mouse mammary carcinoma	4.32 ± 0.72 (3 h)	3.03 ± 0.30 (3 h)	3.22 ± 0.68 (3 h)	Liver-kidney-intestines	(57)
CDF1 mice	C3H mouse mammary carcinoma	5.38 ± 1.95 (2 h)	4.3 ± 2.0 (2 h)	6.4 ± 3.3 (2 h)	Liver-kidney-lung	(49)
Copenhagen rats	Dunning rat R3327-AT prostate carcinoma	0.3 (2 h)				(59)
C3H mice	SCCVII mouse squamous cell carcinoma	1.5 (80 min)				(60)
C3H mice	KHT mouse sarcoma	2.24 ± 0.40 (4 h)		6.79 (4 h)	Liver-large intestine-kidney	(61)
BALB/c	EMT6 mouse breast cancer	3.29 ± 0.73 (30 min)	0.91	1.74	Liver-lung	(50)
Wistar rats	C6 rat glioma	0.42 (2 h)		2.6 (2 h)	Kidney-intestines-liver	(62)
Wistar rats	Walker 256 rat carcinosarcoma	1.00 (3 h)		2.7 ± 0.6 (1 h) 4.4 ± 1.3 (3 h)		(11)
Nude rats	Morris rat McA-R-7777 hepatoma	0.72 (3 h)		2.5 (3 h)		(63)
C3H mice	KHT mouse sarcoma		1.40 ± 0.25 (2 h) 3.30 ± 2.00 (4 h)			(16)
CBA mice	CaNT tumor (Poorly differentiated nonimmunogenic carcinoma)			1.7 ± 0.5	Kidney	(51)
Fisher rats	DMBA induced mammary carcinoma	0.899 ± 0.1132 (1 h) 1.047 ± 0.1107 (2 h) 0.691 ± 0.0967 (2 h)	1.566 ± 0.1879 (1 h) 2.239 ± 0.2042 (2 h) 3.780 ± 0.6762 (4 h)	1.516 ± 0.1754 (1 h) 2.201 ± 0.1576 (2 h) 3.246 ± 0.2994 (4 h)	Liver-kidney	(64)
BALB/c nude mice	A431 human squamous cell carcinoma	3.433 ± 0.770 (3 h)	3.325 ± 0.201 (3 h)	2.764 ± 0.725 (3 h)	Liver-kidney-lung	(65)
BALB/c mice	CT-26 mouse colon carcinoma	4.72 ± 0.25 (10 min) 4.51 ± 0.21 (1 h) 3.85 ± 0.56 (2 h) 3.70 ± 0.34 (2 h)	0.93 ± 0.04 (10 min) 1.30 ± 0.05 (1 h) 1.81 ± 0.19 (2 h) 3.85 ± 0.43 (2 h)	1.06 ± 0.05 (10 min) 1.59 ± 0.11 (1 h) 2.24 ± 0.25 (2 h) 4.42 ± 0.50 (2 h)	Liver-intestines	(66)
[^{18}F]-FAZA						
Swiss nude mice	A431 human epidermoid carcinoma	2.96 ± 1.27 (3 h)	9.62 ± 1.44 (3 h)	7.81 ± 0.94 (3 h)	Liver-kidney-intestines	(57)

Swiss nude mice	AR42J rat pancreatic acinar carcinoma	2.30 ± 1.17 (10 min) 2.87 ± 1.30 (1 h) 1.35 ± 0.89 (3 h)	0.73 ± 0.39 (10 min) 3.27 ± 1.66 (1 h) 9.06 ± 4.07 (3 h)	0.72 ± 0.39 (10 min) 1.69 ± 1.02 (1 h) 5.49 ± 2.26 (3 h)	Kidney-intestines	(57)
BALB/c mice	EMT6 mouse mammary carcinoma	1.38 ± 0.62 (3 h)	9.82 ± 3.94 (3 h)	7.10 ± 2.91 (3 h)	Kidney-intestines	(57)
Wistar rats	Walker 256 rat carcinosarcoma			2.9 ± 0.6 (3 h)		(11)
C3H mice	SCCVII mouse squamous cell carcinoma		1.00 (0.5 h) 1.9 (2 h) 5.8 (4 h)	0.8 (0.5 h) 1.9 (2 h) 6.1 (4 h)		(67)
BALB/c nude mice	A431 human squamous cell carcinoma	1.883 ± 0.170 (3 h)	5.132 ± 0.750 (3 h)	3.050 ± 0.734 (3 h)	Liver-intestine-kidney	(65)
[^{18}F]-FETNIM						
CDF1 mice	C3H mouse mammary carcinoma	3.03 ± 1.32 (2 h)	5.8 ± 2.5 (2 h)	6.2 ± 2.1 (2 h)		(49)
Sprague-Dawley rats	7,12-dimethylbenzanthracene (DMBA) induced mammary carcinoma	0.480 ± 0.10 (15 min) 0.383 ± 0.096 (30 min) 0.239 ± 0.037 (1 h) 0.178 ± 0.046 (2 h) 0.087 ± 0.043 (4 h)	1.49 ± 0.40 (15 min) 1.15 ± 0.35 (30 min) 1.16 ± 0.18 (1 h) 1.79 ± 0.64 (2 h) 1.65 ± 0.87 (4 h)	1.84 ± 0.59 (15 min) 1.11 ± 0.32 (30 min) 0.99 ± 0.16 (1 h) 1.53 ± 0.50 (2 h) 1.42 ± 0.76 (4 h)	Kidney-liver-intestines	(68)
Fischer rats	DMBA induced mammary carcinoma	0.796 ± 0.2036 (1 h) 0.551 ± 0.1582 (2 h) 0.811 ± 0.3377 (4 h)	2.290 ± 0.5994 (1 h) 2.410 ± 0.5672 (2 h) 8.020 ± 2.4200 (4 h)	0.660 ± 0.2666 (1 h) 2.110 ± 0.3468 (2 h) 5.920 ± 2.2400 (4 h)	Kidney-liver	(64)
[^{18}F]-EF3						
C3H mice	FSAII mouse fibrosarcoma	1.11 ± 0.23 (220 min)	2.08 ± 0.18 (220 min)	2.47 ± 0.27 (220 min)	Intestines-kidney-liver	(13)
C3H mice	NF-SA fibrosarcoma	0.78 ± 0.08 (220 min)	1.38 ± 0.15 (220 min)	1.62 ± 0.15 (220 min)		(13)
C3H mice	FSA mouse fibrosarcoma	2.39 ± 0.34 (220 min)	1.24 ± 0.05 (220 min)	1.31 ± 0.04 (220 min)		(13)
C3H mice	SCC VII	1.48 ± 0.16 (220 min)	2.19 ± 0.14 (220 min)	2.55 ± 0.07 (220 min)		(13)
C3H mice	Sa-NH	1.06 ± 0.11 (220 min)	1.97 ± 0.45 (220 min)	2.62 ± 0.24 (220 min)		(13)
C3H mice	MCa-4	1.00 ± 0.29 (220 min)	2.88 ± 0.18 (220 min)	3.52 ± 0.29 (220 min)		(13)
WAG/Rij rats	Rat rhabdomyo-sarcoma R1		2.25 ± 0.09 (3 h) 2.63 ± 0.11 (4 h)			(52)

[^{18}F]-EF5						
Buffalo rats	Morris rat McA-R-7777 hepatoma			1.36-2.34 (3 h)	Intestines-kidney	(14)
Fisher rats	9L rat glioma			0.83-1.48 (3 h)	Intestines-kidney	(14)
[^{18}F]-HX-4						
WAG/Rij rats	Rat rhabdomyo--sarcoma	0.263 ± 0.072 (2 h)[b] 0.227 ± 0.059 (3 h)[b] 0.198 ± 0.048 (4 h)[b] 0.200 ± 0.054 (5 h)[b] 0.181 ± 0.058 (6 h)[b]	1.456 ± 0.270 (2 h) 1.860 ± 0.385 (3 h) 2.512 ± 0.578 (4 h) 2.378 ± 0.557 (5 h) 2.883 ± 0.844 (6 h)		Kidney-bladder	(15)
[^{18}F]FETA						
C3H mice	KHT mouse sarcoma		2.20 ± 0.77 (2 h) 3.84 ± 1.51 (4 h)			(16)
[^{18}F]NEFA						
BALB/c	EMT6 mouse breast cancer	1.55 ± 0.65 (30 min)	0.96	1.14	Liver-lung-kidney	(50)
[^{18}F]NEFT						
BALB/c	EMT6 mouse breast cancer	2.45 ± 0.08 (30 min)	0.98	1. 41	Liver-lung-kidney	(50)
[^{18}F]3-NTR						
CBA mice	CaNT tumor (Poorly differentiated nonimmunogenic carcinoma)			1.6 ± 0.5	Kidney	(51)
Al^{18}F-NODA-ethylnitromidazole						
BALB/c mice	CT-26 mouse colon carcinoma	2.13 ± 0.41 (10 min) 0.24 ± 0.03 (1 h) 0.23 ± 0.05 (2 h)	0.38 (1 h)	14.5 (1 h)	Kidney-liver-lung	(27)
Al^{18}F-NODA-propylnitromidazole						
BALB/c mice	CT-26 mouse colon carcinoma	1.92 ± 0.12 (10 min) 0.33 ± 0.55 (1 h) 0.22 ± 0.04 (2 h)	0.45 (1 h)	3.87 (1 h)	Kidney-liver-lung	(27)

a Data are expressed as mean ± SD. %ID/g, percentage injected dose corrected for weight (g); T/B, tumor-to-blood ratio; T/M, tumor-to-muscle ratio.
b %ID/mL, percentage injected radioactivity per mL

Acknowledgements

This research was supported by National R&D Program through the National Research Foundation of Korea (NRF) funded by the Ministry of Science, ICT & Future Planning (No. 1711026888 and NRF-2016M2C2A1937981) and a grant of the Korea Health Technology R&D Project through the Korea Health Industry Development Institute (KHIDI), funded by the Ministry of Health & Welfare, Republic of Korea (grant number: HI15C3093).

References

1. de Rosales RTM, Årstad E, Blower PJ. Nuclear imaging of molecular processes in cancer. *Targeted Oncol*. 2009;4:183-197.
2. Gambhir SS. Molecular imaging of cancer with positron emission tomography. *Nature Rev Cancer.* 2002;2:683-693.
3. Harry VN, Semple SI, Parkin DE, Gilbert FJ. Use of new imaging techniques to predict tumour response to therapy. *Lancet Oncol.* 2010;11:92-102.
4. Kelloff GJ, Hoffman JM, Johnson B, Scher HI, Siegel BA, Cheng EY, Cheson BD, O'Shaughnessy J, Guyton KZ, Mankoff DA. Progress and promise of FDG-PET imaging for cancer patient management and oncologic drug development. *Clin Cancer Res.* 2005;11:2785-2808.
5. Lehtiö K, Eskola O, Viljanen T, Oikonen V, Grönroos T, Sillanmäki L, Grénman R, Minn H. Imaging perfusion and hypoxia with PET to predict radiotherapy response in head-and-neck cancer. *Int J Radiat Oncol Biol Phys.* 2004;59:971-982.
6. Lucignani G. PET imaging with hypoxia tracers: A must in radiation therapy. *Eur J Nucl Med Mol Imaging.* 2008;35:838-842.
7. Rajendran JG, Schwartz DL, O'Sullivan J, Peterson LM, Ng P, Scharnhorst J, Grierson JR, Krohn KA. Tumor hypoxia imaging with [F-18] fluoromisonidazole positron emission tomography in head and neck cancer. *Clin Cancer Res.* 2006;12:5435-5441.
8. Koh W-J, Rasey JS, Evans ML, Grierson JR, Lewellen TK, Graham MM, Krohn KA, Griffin TW. Imaging of hypoxia in human tumors with [F-18] fluoromisonidazole. *Int J Radiat Oncol Biol Phys.* 1992;22:199-212.
9. Valk PE, Mathis CA, Prados MD, Gilbert JC, Budinger TF. Hypoxia in human gliomas: Demonstration by PET with fluorine-18-fluoromisonidazole. *J Nucl Med.* 1992;33:2133-2137.
10. Gomez FLG, Uehara T, Rokugawa T, Higaki Y, Suzuki H, Hanaoka H, Akizawa H, Arano Y. Synthesis and evaluation of diastereoisomers of 1,4,7-triazacyclononane-1, 4,7-tris-(glutaric acid) (NOTGA) for multimeric radiopharmaceuticals of gallium. *Bioconjug Chem.* 2012;23:2229-2238.
11. Sorger D, Patt M, Kumar P, Wiebe LI, Barthel H, Seese A, Dannenberg C, Tannapfel A, Kluge R, Sabri O. [18F] Fluoroazomycinarabinofuranoside (18FAZA) and [18F] Fluoromisonidazole (18FMISO): A comparative study of their selective uptake in hypoxic cells and PET imaging in experimental rat tumors. *Nucl Med Biol.* 2003;30:317-326.
12. Kachur AV, Dolbier Jr WR, Evans SM, Shiue C-Y, Shiue GG, Skov KA, Baird IR, James BR, Li A-R, Roche A, Koch CJ. Synthesis of new hypoxia markers EF1 and [^{18}F]-EF1. *Appl Radiat Isot.* 1999;51:643-650.
13. Mahy P, De Bast M, Leveque P, Gillart J, Labar D, Marchand J, Grégoire V. Preclinical validation of the hypoxia tracer 2-(2-nit roimidazol-1-yl)-N-(3, 3, 3-[^{18}F] trifluoropropyl) acetamide,[^{18}F] EF3. *Eur J Nucl Med Mol Imaging.* 2004;31:1263-1272.
14. Ziemer L, Evans S, Kachur A, Shuman A, Cardi C, Jenkins W, Karp J, Alavi A, Dolbier W, Koch C. Noninvasive imaging of tumor hypoxia in rats using the 2-nitroimidazole 18F-EF5. *Eur J Nucl Med Mol Imaging.* 2003;30:259-266.
15. Dubois LJ, Lieuwes NG, Janssen MHM, Peeters WJM, Windhorst AD, Walsh JC, Kolb HC, Öllers MC, Bussink J, Van Dongen GAMS, Van Der Kogel A, Lambin P. Preclinical evaluation and validation of [^{18}F]HX4,a promising hypoxia marker for imaging. *Proc Nat Acad Sci.* 2011;108:14620-14625.
16. Rasey JS, Hofstrand PD, Chin LK, Tewson TJ. Characterization of [18F] fluoroetanidazole, a new radiopharmaceutical for detecting tumor hypoxia. *J Nucl Med.* 1999;40:1072.
17. Hoigebazar L, Jeong JM. Hypoxia Imaging Agents Labeled with Positron Emitters. *Recent Results Cancer Res.* 2013;194:285-299.
18. Kelada OJ, Carlson DJ. Molecular imaging of tumor hypoxia with positron emission tomography. *Radiat Res.* 2014;181:335-349.
19. Kizaka-Kondoh S, Konse-Nagasawa H. Significance of nitroimidazole compounds and hypoxia-inducible factor-1 for imaging tumor hypoxia. *Cancer Sci.* 2009;100:1366-1373.
20. Nunn A, Linder K, Strauss HW. Nitroimidazoles and imaging hypoxia. *Eur J Nucl Med.* 1995;22:265-280.
21. Rauth A, Melo T, Misra V. Bioreductive therapies: an overview of drugs and their mechanisms of action. *Int J Radiat Oncol Biol Phys.* 1998;42:755-762.
22. Takasawa M, Moustafa RR, Baron J-C. Applications of nitroimidazole in vivo hypoxia imaging in ischemic *stroke.* Stroke. 2008;39:1629-1637.
23. Dubois L, Landuyt W, Haustermans K, Dupont P, Bormans G, Vermaelen P, Flamen P, Verbeken E, Mortelmans L. Evaluation of hypoxia in an experimental

rat tumour model by 18F Fluoromisonidazole PET and immunohistochemistry. *Br J Ca.* 2004;91:1947-1954.
24. Tang G, Wang M, Tang X, Gan M, Luo L. Fully automated one-pot synthesis of [^{18}F] fluoromisonidazole. *Nucl Med Biol* 2005;32:553-558.
25. Kumar P, Stypinski D, Xia H, McEwan AJB, Machulla HJ, Wiebe LI. Fluoroazomycin arabinoside (FAZA): Synthesis, 2H and 3H-labelling and preliminary biological evaluation of a novel 2-nitroimidazole marker of tissue hypoxia. *J Label Compd Radiopharm.* 1999;42:3-16.
26. Wiebe L. Radiohalogenated nitroimidazoles for single-photon scintigraphic imaging of hypoxic tissues. in Imaging of hypoxia: Tracer developments. Vol. 33, Ed. Machulla H-J. Springer Science & Business Media; 1999, pp155-169.
27. Hoigebazar L, Jeong JM, Lee JY, Shetty D, Yang BY, Lee YS, Lee DS, Chung JK, Lee MC. Syntheses of 2-nitroimidazole derivatives conjugated with 1,4,7-triazacyclononane-N, N ′-diacetic acid labeled with F-18 using an aluminum complex method for hypoxia imaging. *J Med Chem.* 2012;55:3155-3162.
28. Shetty D, Choi SY, Jeong JM, Lee JY, Hoigebazar L, Lee YS, Lee DS, Chung JK, Lee MC, Chung YK. Stable aluminium fluoride chelates with triazacyclononane derivatives proved by X-ray crystallography and ^{18}F-labeling study. *Chem Commun.* 2011;47:9732-9734.
29. Shetty D, Jeong JM, Kim YJ, Lee JY, Hoigebazar L, Lee Y-S, Lee DS, Chung J-K. Development of a bifunctional chelating agent containing isothiocyanate residue for one step F-18 labeling of peptides and application for RGD labeling. *Bioorg. Med. Chem.* 2012;20:5941-5947.
30. Hoigebazar L, Jeong JM, Choi SY, Choi JY, Shetty D, Lee Y-S, Lee DS, Chung J-K, Lee MC, Chung YK. Synthesis and characterization of nitroimidazole derivatives for 68Ga-labeling and testing in tumor xenografted mice. *J Med Chem.* 2010;53:6378-6385.
31. Hoigebazar L, Jeong JM, Hong MK, Kim YJ, Lee JY, Shetty D, Lee YS, Lee DS, Chung JK, Lee MC. Synthesis of 68Ga-labeled DOTA-nitroimidazole derivatives and their feasibilities as hypoxia imaging PET tracers. *Bioorg Med Chem.* 2011;19:2176-2181.
32. Kizaka-Kondoh S, Inoue M, Harada H, Hiraoka M. Tumor hypoxia: A target for selective cancer therapy. *Cancer Sci.* 2003;94:1021-1028.
33. Aboagye E, Lewis A, Johnson A, Workman P, Tracy M, Huxham I. The novel fluorinated 2-nitroimidazole hypoxia probe SR-4554: Reductive metabolism and semiquantitative localisation in human ovarian cancer multicellular spheroids as measured by electron energy loss spectroscopic analysis. *Br J Ca.* 1995;72:312-318.
34. Linder KE, Chan YW, Cyr JE, Malley MF, Nowotnik DP, Nunn AD. TcO (PnAO-1-(2-nitroimidazole))[BMS-181321], a new technetium-containing nitroimidazole complex for imaging hypoxia: synthesis, characterization, and xanthine oxidase-catalyzed reduction. *J Med Chem.* 1994;37:9-17.
35. Chu T, Hu S, Wei B, Wang Y, Liu X, Wang X. Synthesis and biological results of the technetium-99m-labeled 4-nitroimidazole for imaging tumor hypoxia. *Bioorg Med Chem Lett.* 2004;14:747-749.
36. Li Z, Zhang J, Jin Z, Zhang W, Zhang Y. Synthesis and biodistribution of novel 99mTc labeled 4-nitroimidazole dithiocarbamate complexes as potential agents to target tumor hypoxia. *Med Chem Comm.* 2015;6:1143-1148.
37. Barthel H, Wilson H, Collingridge D, Brown G, Osman S, Luthra S, Brady F, Workman P, Price PM, Aboagye E. In vivo evaluation of ^{18}F fluoroetanidazole as a new marker for imaging tumour hypoxia with positron emission tomography. *Br J Ca.* 2004;90:2232-2242.
38. Lee ST, Scott AM. Hypoxia positron emission tomography imaging with ^{18}F-fluoromisonidazole. *Semin Nucl Med.* 2007:37:451-461.
39. Martin GV, Caldwell JH, Rasey JS, Grunbaum Z, Cerqueira M, Krohn KA. Enhanced binding of the hypoxic cell marker [^{3}H] fluoromisonidazole in ischemic myocardium. *J Nucl Med.* 1989;30:194-201.
40. Rasey JS, Koh W-j, Evans ML, Peterson LM, Lawellen TK, Graham MM, Krohn KA. Quantifying regional hypoxia in human tumors with positron emission tomography of [^{18}F] fluoromisonidazole: a pretherapy study of 37 patients. *Int J Radiat Oncol Biol Phys.* 1996;36:417-428.
41. Bruehlmeier M, Roelcke U, Schubiger PA, Ametamey SM. Assessment of hypoxia and perfusion in human brain tumors using PET with ^{18}F-fluoromisonidazole and ^{15}O-H2O. *J Nucl Med.* 2004;45:1851-1859.
42. Eschmann S-M, Paulsen F, Reimold M, Dittmann H, Welz S, Reischl G, Machulla H-J, Bares R. Prognostic impact of hypoxia imaging with ^{18}F-misonidazole PET in non-small cell lung cancer and head and neck cancer before radiotherapy. *J Nucl Med.* 2005;46:253-260.
43. Guadagno JV, Donnan GA, Markus R, Gillard JH, Baron J-C. Imaging the ischaemic penumbra. *Curr Opin Neurol.* 2004;17:61-67.
44. Markus R, Reutens D, Kazui S, Read S, Wright P, Pearce DC, Tochon-Danguy H, Sachinidis J, Donnan G. Hypoxic tissue in ischaemic stroke: Persistence and clinical consequences of spontaneous survival. *Brain.* 2004;127:1427-1436.
45. Kubota K, Tada M, Yamada S, Hori K, Saito S, Iwata R, Sato K, Fakuda H, Ido T. Comparison of the distribution of fluorine-18 fluoromisonidazole, deoxyglucose and methionine in tumour tissue. *Eur J Nucl Med.* 1999;26:750-757.
46. Mahy P, De Bast M, de Groot T, Cheguillaume A, Gillart J, Haustermans K, Labar D, Grégoire V. Comparative pharmacokinetics, biodistribution, metabolism and hypoxia-

dependent uptake of [18F]-EF3 and [18F]-MISO in rodent tumor models. *Radiother Oncol.* 2008;89:353-360.
47. Krohn KA, Link JM, Mason RP. Molecular Imaging of Hypoxia. *J Nucl Med.* 2008;49(Suppl 2):129S-48S.
48. Chitneni SK, Palmer GM, Zalutsky MR, Dewhirst MW. Molecular imaging of hypoxia. *J Nucl Med.* 2011;52:165-168.
49. Grönroos T, Bentzen L, Marjamäki P, Murata R, Horsman MR, Keiding S, Eskola O, Haaparanta M, Minn H, Solin O. Comparison of the biodistribution of two hypoxia markers [18F] FETNIM and [18F] FMISO in an experimental mammary carcinoma. *Eur J Nucl Med Mol Imaging.* 2004;31:513-520.
50. Zha Z, Zhu L, Liu Y, Du F, Gan H, Qiao J, Kung HF. Synthesis and evaluation of two novel 2-nitroimidazole derivatives as potential PET radioligands for tumor imaging. *Nucl Med Biol.* 2011;38:501-508.
51. Bejot R, Kersemans V, Kelly C, Carroll L, King RC, Gouverneur V. Pre-clinical evaluation of a 3-nitro-1, 2, 4-triazole analogue of [18F] FMISO as hypoxia-selective tracer for PET. *Nucl Med Biol.* 2010;37:565-575.
52. Dubois L, Landuyt W, Cloetens L, Bol A, Bormans G, Haustermans K, Labar D, Nuyts J, Grégoire V, Mortelmans L. [18F] EF3 is not superior to [18F] FMISO for PET-based hypoxia evaluation as measured in a rat rhabdomyosarcoma tumour model. *Eur J Nucl Med Mol Imaging.* 2009;36:209-218.
53. Busch TM, Hahn SM, Evans SM, Koch CJ. Depletion of tumor oxygenation during photodynamic therapy: detection by the hypoxia marker EF3 [2-(2-nitroimidazol-1 [H]-yl)-N-(3, 3, 3-trifluoropropyl) acetamide]. *Cancer Res.* 2000;60:2636-2642.
54. Koch CJ. [1] Measurement of absolute oxygen levels in cells and tissues using oxygen sensors and 2-nitroimidazole EF5. *Methods Enzymol.* 2002;352:3-31.
55. Troost EG, Laverman P, Kaanders JH, Philippens M, Lok J, Oyen WJ, van der Kogel AJ, Boerman OC, Bussink J. Imaging hypoxia after oxygenation-modification: comparing [18F] FMISO autoradiography with pimonidazole immunohistochemistry in human xenograft tumors. *Radiother Oncology.* 2006;80:157-164.
56. Fleming IN, Manavaki R, Blower PJ, West C, Williams KJ, Harris AL, Domarkas J, Lord S, Baldry C, Gilbert FJ. Imaging tumour hypoxia with positron emission tomography. *Br J Ca.* 2015;112:238-250.
57. Piert M, Machulla H-J, Picchio M, Reischl G, Ziegler S, Kumar P, Wester HJ, Beck R, McEwan AJ, Weibe LI. Hypoxia-specific tumor imaging with 18F-fluoroazomycin arabinoside. *J Nucl Med.* 2005;46:106-113.
58. Wyss MT, Honer M, Schubiger PA, Ametamey SM. NanoPET imaging of [18F] fluoromisonidazole uptake in experimental mouse tumours. *Eur J Nucl Med Mol Imaging.* 2006;33:311-318.
59. Cho H, Ackerstaff E, Carlin S, Lupu ME, Wang Y, Rizwan A, O'Donoghue J, Ling CC, Humm JL, Zanzonico PB. Noninvasive multimodality imaging of the tumor microenvironment: registered dynamic magnetic resonance imaging and positron emission tomography studies of a preclinical tumor model of tumor hypoxia. *Neoplasia.* 2009;11:247-259.
60. Sorensen M, Horsman MR, Cumming P, Munk OL, Keiding S. Effect of intratumoral heterogeneity in oxygenation status on FMISO PET, autoradiography, and electrode Po2 measurements in murine tumors. *Int J Radiat Oncol Biol Phys.* 2005;62:854-861.
61. Liu RS, Chou TK, Chang CH, Wu CY, Chang CW, Chang TJ, Wang SJ, Lin WJ, Wang HE. Biodistribution, pharmacokinetics and PET imaging of [18F]FMISO, [18F] FDG and [18F]FAc in a sarcoma- and inflammation-bearing mouse model. *Nucl Med Biol.* 2009;36:305-312.
62. Tochon-Danguy HJ, Sachinidis JI, Chan F, Chan JG, Hall C, Cher L, Stylli S, Hill J, Kaye A, Scott AM. Imaging and quantitation of the hypoxic cell fraction of viable tumor in an animal model of intracerebral high grade glioma using [18F]fluoromisonidazole (FMISO). *Nucl Med Biol.* 2002;29:191-197.
63. Riedl CC, Brader P, Zanzonico P, Reid V, Woo Y, Wen B, Ling CC, Hricak H, Fong Y, Humm JL. Tumor hypoxia imaging in orthotopic liver tumors and peritoneal metastasis: a comparative study featuring dynamic 18F-MISO and 124IIAZG PET in the same study cohort. *Eur J Nucl Med Mol Imaging.* 2008;35:39-46.
64. Yang DJ, Wallace S, Cherif A, Li C, Gretzer MB, Kim EE, Podoloff DA. Development of F-18-labeled fluoroerythronitroimidazole as a PET agent for imaging tumor hypoxia. *Radiology.* 1995;194:795-800.
65. Reischl G, Dorow DS, Cullinane C, Katsifis A, Roselt P, Binns D, Hicks RJ. Imaging of tumor hypoxia with [124I] IAZA in comparison with [18F]FMISO and [18F]FAZA-first small animal PET results. *J Pharm Pharma Sci.* 2007;10:203-211.
66. Seelam SR, Lee JY, Kim YJ, Lee Y-S, Jeong JM. Biodistribution and PET imaging of [18F]FMISO in mousecolon cancer xenografted mice. *J Radiopharm Mol Prob.* 2015;1:137-144.
67. Busk M, Horsman MR, Jakobsen S, Hansen KV, Bussink J, van der Kogel A, Overgaard J. Can hypoxia-PET map hypoxic cell density heterogeneity accurately in an animal tumor model at a clinically obtainable image contrast? *Radiother Oncology.* 2009;92:429-436.
68. Gronroos T, Eskola O, Lehtio K, Minn H, Marjamaki P, Bergman J, Haaparanta M, Forsback S, Solin O. Pharmacokinetics of [18F]FETNIM: A potential marker for PET. *J Nucl Med.* 2001;42(9):1397-1404.